metals

Article

Test on Compressive Performance of Hollow Concrete-Filled Sandwich Circular Steel Tubes Connected by Thread

Qingli Wang [1,*], Jie Zhao [1] and Kuan Peng [2]

[1] School of Civil Engineering, University of Science and Technology Liaoning, Anshan 114044, China; zj1231230303@163.com
[2] School of Mechatronic Engineering, Southwest Petroleum University, Chengdu 610500, China; pklut7@163.com
* Correspondence: 320183700100@ustl.edu.cn

Abstract: The connection method of lengthening the steel tube of hollow concrete-filled sandwich circular steel tubes and threaded connections is proposed. The length, depth and position are the basic parameters. Twelve hollow concrete sandwich circular steel pipes with threaded connections were designed and subjected to axial compression tests. The axial compressive loading–longitudinal compressive displacement curves, axial compressive loading strain of steel tube curves and failure mode of the specimens are analyzed, and the effects of different parameters on the axial compressive-bearing capacity and stiffness of the specimens are studied. The results showed that within the range of parameters studied, the axial compression load–longitudinal compression displacement curves of the specimens were the linear elastic stage and the elastic–plastic stage, which can be divided into a yield-strengthening stage and a decreasing stage. The bearing capacity and strength of the lined threaded connection specimen are not inferior to those of the ordinary specimen or the welded specimen. The bearing capacity and strength of the specimen increase with the increase of the thread length. The bearing capacity and strength of the specimens connected with inner liner screws at the ends are higher than those connected with inner liner bolts at the middle.

Keywords: hollow concrete-filled sandwich circular steel tube; axial compressive performance; thread connection; inner lining tube; load-bearing capacity

Citation: Wang, Q.; Zhao, J.; Peng, K. Test on Compressive Performance of Hollow Concrete-Filled Sandwich Circular Steel Tubes Connected by Thread. *Metals* **2023**, *13*, 1207. https://doi.org/10.3390/met13071207

Academic Editor: Elide Elide Nastri

Received: 17 May 2023
Revised: 15 June 2023
Accepted: 25 June 2023
Published: 29 June 2023

1. Introduction

Hollow concrete-filled sandwich steel tube structures have the characteristics of light weight, high fire resistance and good economic effect [1], and their internal space can be used to lay water tubes and electricity pipelines. Compared with solid concrete-filled steel tubular structures, they have good functional expansibility [2], and in recent years have been more applied and studied in the field of engineering [3].

Steel pipe lengthening often occurs in engineering [4]. Weld, grouting sleeve connections and flange connections have always been used [5], as shown in Figure 1.

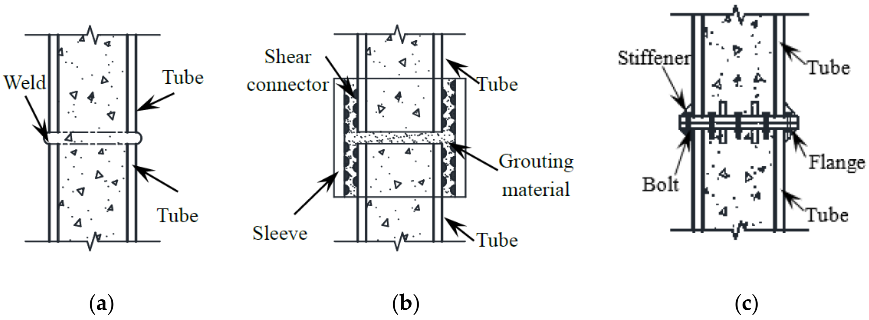

Figure 1. Common lengthening methods of steel tube of concrete-filled steel tube: (**a**) welding, (**b**) grouting sleeve connection, (**c**) flange connection.

Welding is currently an important method of connecting steel structures, but there are still some quality issues due to manual welding [6,7]. Hao [8] summarized the research results of the failure modes of grouted casing under different environments. The results show that a grouted casing connection has high bearing capacity and good ductility under static loads. The hysteretic ring is full and has good energy dissipation capacity under low cycle reciprocating loads. It can still maintain good ductility under fire. Sun [9] studied the factors affecting the bearing capacity of a new type of grouting sleeve connection device, and designed and made 27 test members for tensile tests. The test results show that the axial force of the device is mainly transmitted by the high-strength grouting material poured in the space between the steel pipes. The ultimate bearing capacity of the grouting sleeve increases with the increase of the strength of the grouting material. The ultimate bearing capacity of the grouting sleeve increases with the increase of the anchorage length. Wang [10] studied the bending performance of hollow sandwich concrete-filled circular steel tubular internal and external flange connections through finite element simulation analysis. The results show that the bending capacity of the joints is mainly borne by the tension of the internal and external bolts, which is specifically manifested by the necking and tensile failure of the bolts in the tension zone, and the tension provided by the concrete is relatively small. Yi [11] studied the mechanical properties of the internal and external flange joints of conical members under bending and axial tension through finite-element analysis. The results show that the bending and tensile capacity of the joints are mainly borne by the internal and external bolts, and the bending members are specifically represented by the necking and tensile failure of the bolts in the tension zone. The practical calculation method of the bolt tension of the member node is preliminarily determined. In addition, there are many newer connection methods. Deng et al. [12]. designed a new type of stiffening flange connection for large circular hollow section (CHS)—internal and external double layer (IODL) flange connection. This connection method fully utilizes the internal space of the circular pipe, and uses smaller bolts and thinner flanges. Through tensile and compressive tests, it is proved that the structure has good ductility and can meet the safety requirements of engineering practice. Grundy P et al. [13] conducted chemical prestressing tests using expansive agents in grouted pile sleeve connections, indicating that the enhanced bond of this structure is more predictable than that of conventional grouted pile sleeve connections and can significantly improve the shear bond strength. This allows for shorter design lengths and improves efficiency under static and cyclic loading. Zhai [14] proposed two construction methods for splicing concrete-filled steel tubular columns connected with inner sleeves, through flange connections and bolt connections. Eight specimens were designed and fabricated to conduct axial compression performance tests. The tests show that the two types of concrete-filled steel tubular column-splicing structures can meet the requirements of concrete-filled steel tubular column- to-column connection joints. Yang [15] proposed a method for assembling concrete-filled steel tubular column steel beam connections based on flange connections and external stiffening rings, characterized by the use of high-strength bolts, rigid flanges, and external stiffening ring plates at the same location to achieve concrete-filled steel tubular column-to-column connections, and concrete-filled steel tubular column to steel beam connections. The research results show that the flange-connected concrete-filled steel tubular column steel beam reinforced ring joints have good seismic performance. The width of the stiffening ring plate is an important factor affecting its mechanical performance. The improved design method of the outer stiffening ring plate can reasonably consider the contribution of the flange and the impact of the discontinuity of the column steel tube at the joint. Wang [16] conducted axial tensile tests on nine concrete-filled circular steel tubular members with internal lattice angle steel, and studied the impact of the connection methods of the outer steel pipe and the inner angle steel on the axial tensile properties of the members. The results show that the connection mode of an outer steel pipe and inner angle steel has no effect on the axial tensile performance and bearing capacity of the component, but does impact the initial stiffness of the component. Welding stiffening ribs at the end of the outer steel pipe can significantly improve the bearing capacity of the internal angle steel skeleton of the component. In order to avoid the disadvantages of the above steel structure connection method, a threaded connection method of the inner liner pipe is proposed.

2. Specimen Design and Raw Material Performance

2.1. Specimen Design

Fifteen concrete-filled steel tube specimens were designed, including hollow sandwich concrete-filled steel tube specimens, welded joints between concrete-filled steel tube specimens and ordinary concrete-filled steel tube specimens. The length of the specimen L = 399 mm, the diameter of the outer steel tube D_{os} = 133 mm, the diameter of inner steel tube D_{is} = 76 mm, the wall thickness of the outer steel tube t_{os} and wall thickness of the inner steel tube t_{is} are 6 mm, and the wall thickness of the outer tube of inner lining tube t_{ois} and the wall thickness of the inner tube of inner lining tube t_{iis} are 8 mm. The thread length l is taken as $D_{os}/2$, $D_{os}/4$ and $D_{os}/8$. The thread depth h is taken as $0.1t_{os}$ and $0.15t_{os}$, respectively. The thread error is less than 2.6% for a thread depth of 0.6 mm and less than 2.1% for a thread depth of 0.9 mm. All parameters of CFST specimens are shown in Table 1.

Table 1. Parameters of specimens.

No.	Weld/Thread Position	*h*/mm	*l*/mm
C	–	–	–
MW	Middle section	–	–
EW	End section	–	–
M6A	Middle section	0.6	16.5
M6B	Middle section	0.6	33
M6C	Middle section	0.6	66
M9A	Middle section	0.9	16.5
M9B	Middle section	0.9	33
M9C	Middle section	0.9	66
E6A	End section	0.6	16.5
E6B	End section	0.6	33
E6C	End section	0.6	66
E9A	End section	0.9	16.5
E9B	End section	0.9	33
E9C	End section	0.9	66

The hollow ratio χ [17] is 0.628, and the confinement effect coefficient ξ [18] of the specimens is 2.33. The calculation of these parameters is as follows:

$$\chi = D_{is}/(D_{os} - 2t_{os}) \tag{1}$$

$$\xi = (A_s f_y)/(A_c f_{ck}) \tag{2}$$

$$f_{ck} = 0.67 f_{cu} \tag{3}$$

where A_s is the cross-sectional area of steel tube, f_y is the yield strength of steel tube, A_c is the cross-sectional area of concrete, f_{ck} is the characteristic axial compressive strength of concrete, and f_{cu} is the cubic compressive strength of concrete.

2.2. Material Properties

The performance indices of steel are shown in Table 2.

In addition, the compressive strength of concrete is f_{cu} = 56 MPa, and the elastic modulus of concrete is E_c = 35.512 GPa.

Table 2. Performance indices of steel.

Type	f_y/MPa	f_u/MPa	E_s/GPa	v_s	δ
Outer steel tube	420	570	215	0.28	20.7
Outer inner lining tube	419	569	210	0.27	25.9
Inner steel tube	509	624	211	0.23	21.3
Inner inner lining tube	396	517	207	0.27	21.0

2.3. Preparation of Specimens

The detailed drawings of some specimens are shown in Figure 2, in which the unit of dimensions is mm.

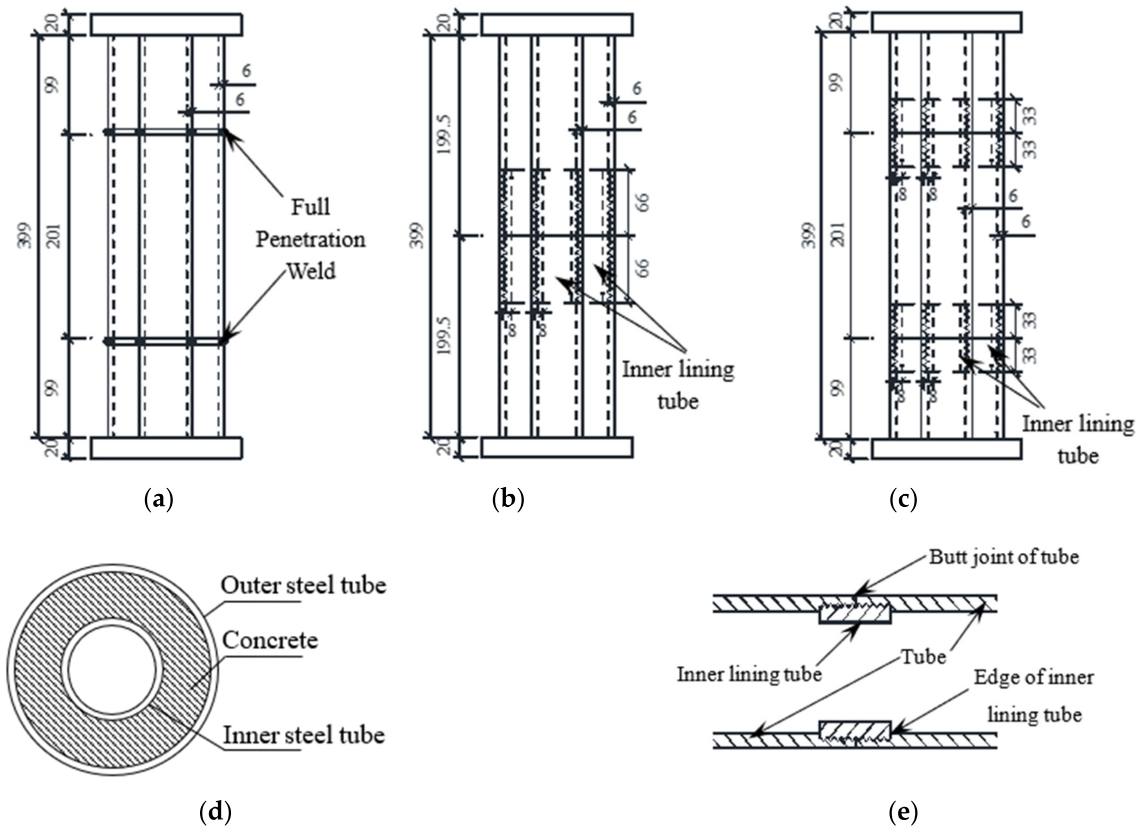

Figure 2. Schematic diagram of steel components of some specimens: (**a**) specimen EW; (**b**) specimen M6C/M9C; (**c**) specimen E6B/E9B; (**d**) Cross-section; (**e**) Steel tube lengthened by thread through inner lining tube.

In order to more clearly display the assembly figure of the hollow concrete-filled sandwich circular steel tube connected by thread, Figure 3 shows the partial diagram of some specimen components of the threaded connection specimen of the inner liner and the partial specimen assembly diagram. All specimens after preparation are shown in Figure 4.

2.4. Loading and Measurement

The test equipment is shown in Figure 5. Four displacement meters were arranged around the sample at 90° intervals, and a transverse strain gauge and a longitudinal strain gauge were pasted to the outer wall of the steel pipe at 90° intervals.

(**a**)

(**b**)

Figure 3. Actual machining figure of steel components of some specimens. (**a**) Partial diagram of some specimen components; (**b**) Partial specimen assembly diagram.

Figure 4. All specimens before test.

Figure 5. Test equipment.

The sample was preloaded first [19–22]. The entire loading process adopted the method of load controlled. Within the elastic range, the loading of each stage was 1/10 of the estimated bearing capacity, the instrument data were recorded after each stage of loading, and the next stage of loading was carried out after holding the load for 2 min until it reached 60% of the estimated bearing capacity. Then, loading took place at the rate of 2 kN/s, and the loading stage was stopped when the compressive displacement reached 30 mm (about 75,000 $\mu\varepsilon$).

3. Specimen Failure Model

3.1. Outer Steel Tube

The failure of the outer steel tube mainly shows three modes. The first mode (Outer I) corresponds to C, MW and EW specimens and shows the outward buckling deformation of the outer steel pipe bounded by the end plate and the weld in Figure 6. This is due to the high strength of the weld lines and the end effect [18].

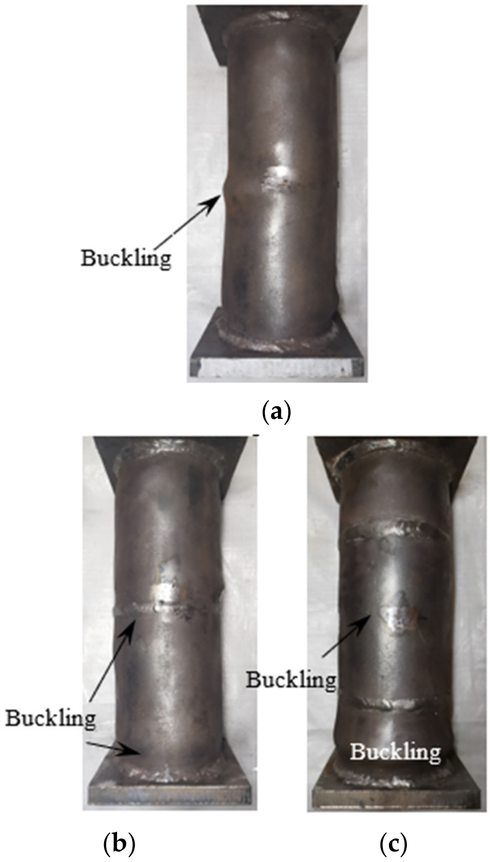

Figure 6. Failure modes of outer steel tube of common specimen and welded specimen. (**a**) Specimen C; (**b**) Specimen MW; (**c**) Specimen EW.

The second mode (Outer II) corresponds to the specimens with short inner lining tubes (specimen M6A, M9A, E6A and E9A), which shows that in addition to the outward buckling caused by the end effect, outward buckling also occurs at one of the weak positions of the specimen, i.e., the butt joint of the tube (Figure 2), as shown in Figure 7.

The third mode (Outer III) corresponds to the specimens with long inner lining tubes (specimen M6B, M9B, E6C and E9C, etc.), which shows that, in addition to the outward buckling caused by the end effect, outward buckling occurs at one of the weak positions of the specimen, as shown in Figure 8.

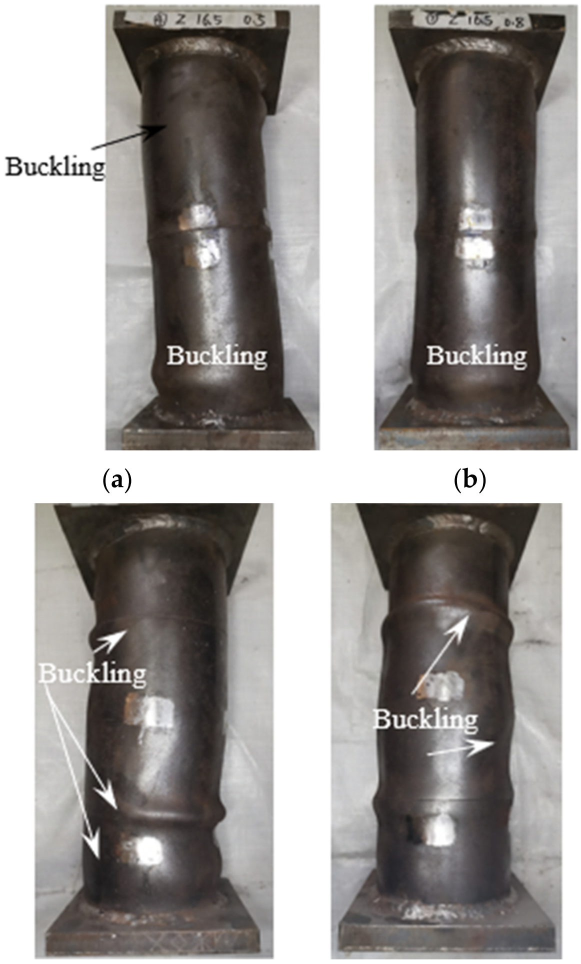

(c) (d)

Figure 7. Second type of failure mode of outer steel tube. (**a**) Specimen M6A; (**b**) Specimen M9A; (**c**) Specimen E6A; (**d**) Specimen E9A.

3.2. Inner Steel Tube

The failure modes of the inner steel tube are also divided into three types. The first (Inner I) failure mode corresponds to the Outer I failure mode, such as specimens C and WM, in which the position of outward buckling of the inner steel tube corresponds to the position of outward buckling at the end of the outer steel tube, and the inward concavity of inner steel tube corresponds to the outward buckling of the outer steel tube at the other position, as shown in Figure 9.

The second mode (Inner II) corresponds to the Outer II failure mode. The outward buckling of the inner steel pipe corresponds to the outward buckling of the end of the outer steel pipe, as shown in Figure 10a. Corresponding to the outward buckling at the other position of the outer steel tube, the inner steel tube has no obvious deformation, although the edge of the inner lining tube has outward buckling (Figure 10b).

The third mode (Inner III) corresponds to the Outer III failure mode. The outward buckling of the inner steel pipe corresponds to the outward buckling of the end of the outer steel pipe, as shown in Figure 11a. Corresponding to the outward buckling at the edge of the inner lining tube of the outer steel tube, the inner steel tube of the same section has no obvious deformation, although outward buckling occurs at the nearby inner steel tube (Figure 11).

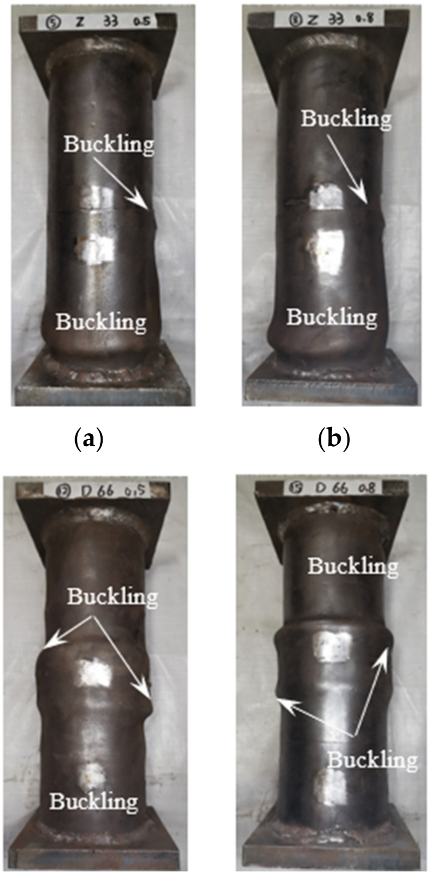

(**a**) (**b**)

(**c**) (**d**)

Figure 8. Third type of failure mode of outer steel tube. (**a**) Specimen M6B; (**b**) Specimen; M9B (**c**) Specimen E6C; (**d**) Specimen E9C.

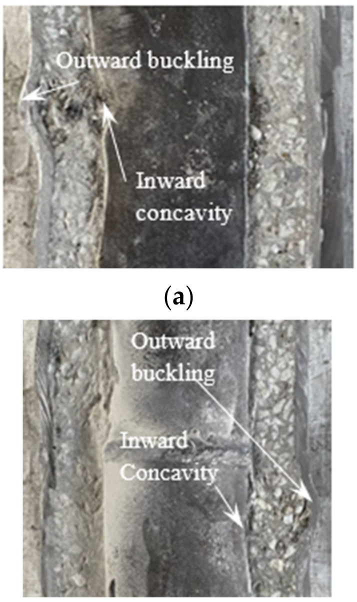

(**a**)

(**b**)

Figure 9. Failure modes of inner steel tube of common specimen and welded specimen. (**a**) Specimen C; (**b**) Specimen MW.

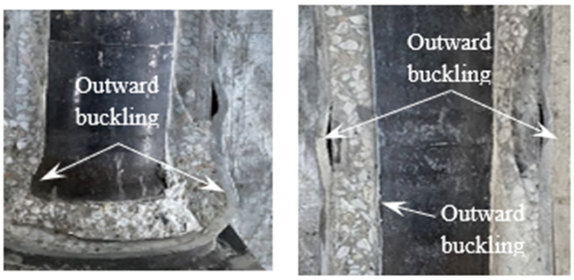

(a) (b)

Figure 10. Second type of failure mode of inner steel tube. (**a**) specimen M6A; (**b**) specimen M9A.

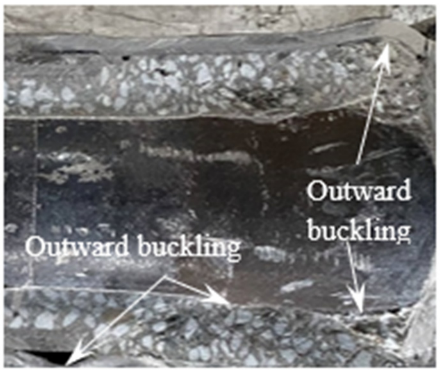

(**a**)

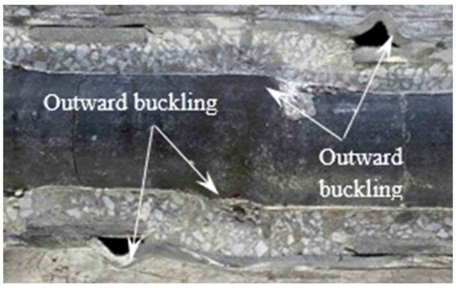

(**b**)

Figure 11. Third type of failure mode of inner steel tube. (**a**) Specimen E9B; (**b**) Specimen M6B.

3.3. Concrete

The failure mode of concrete is shown in Figure 12. It can be seen that the crushed or buckling of concrete corresponds to the steel tube buckling.

(**a**)

Figure 12. *Cont.*

(**b**)

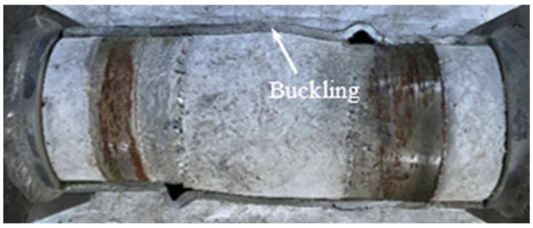

(**c**)

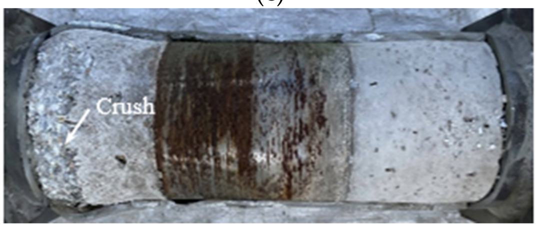

(**d**)

Figure 12. Failure modes of concrete. (**a**) Specimen C; (**b**) Specimen MW; (**c**) Specimen E9B; (**d**) Specimen M9C.

4. Curve Analysis

4.1. N-Δ Curve

As can be seen from Figure 13, the bearing capacity and stiffness of welded specimens are basically the same as those of ordinary specimens, and the welding position has little impact on the bearing capacity and hardness. This indicates that the welding effect is good and can basically meet the use requirements of ordinary specimens.

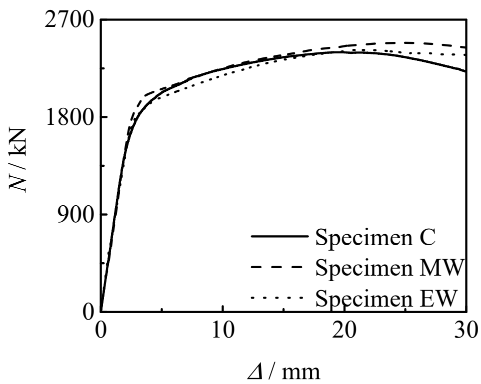

Figure 13. *N*-Δ curves of ordinary specimens and welded specimens.

As can be seen from Figure 14, the bearing capacity and stiffness of threaded connection specimens are basically consistent with those of welded specimens. This indicates that this connection method has a good effect, and the steel pipe still has a good constraint effect on the concrete. It can also be seen that the curve has a downward section. The curve trend of the sample is consistent with the results of the references [19,20].

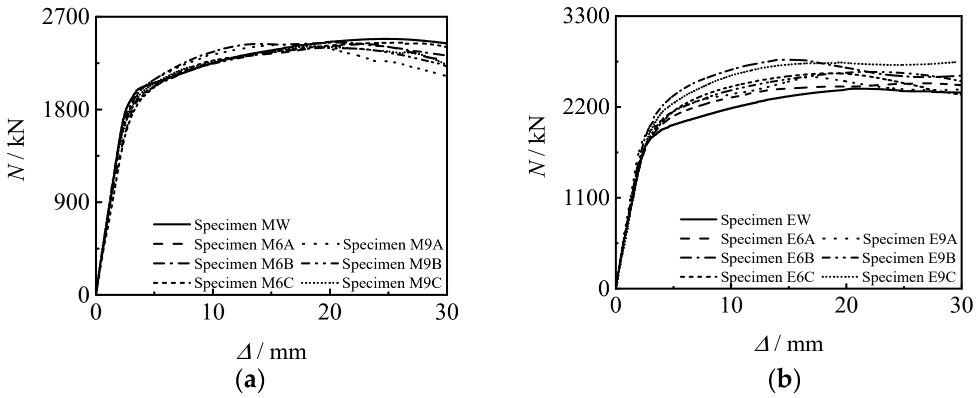

Figure 14. *N*-Δ curves of connected specimens: (**a**) middle section; (**b**) end section.

4.2. N-Steel Tube Strain (ε_s) Curve

Figure 15 shows the N-ε_s curve of all specimens. It can be seen that the trend of all curves is similar, with steel pipes being compressed in the longitudinal direction and stretched in the transverse direction. Due to the small longitudinal strain, the Poisson's ratio of the steel tube is usually constant, indicating that there is no interaction between the steel tube and the concrete at this time. With the increase of longitudinal strain, the Poisson's ratio of concrete increases, indicating that the concrete gradually contacts the steel pipe. When the curve reaches the descending section, the lateral strain of the steel pipe increases significantly due to the increased restraint of the steel pipe on the concrete. Therefore, the pipe specimen connected through the inner thread still has good mechanical properties [21–23].

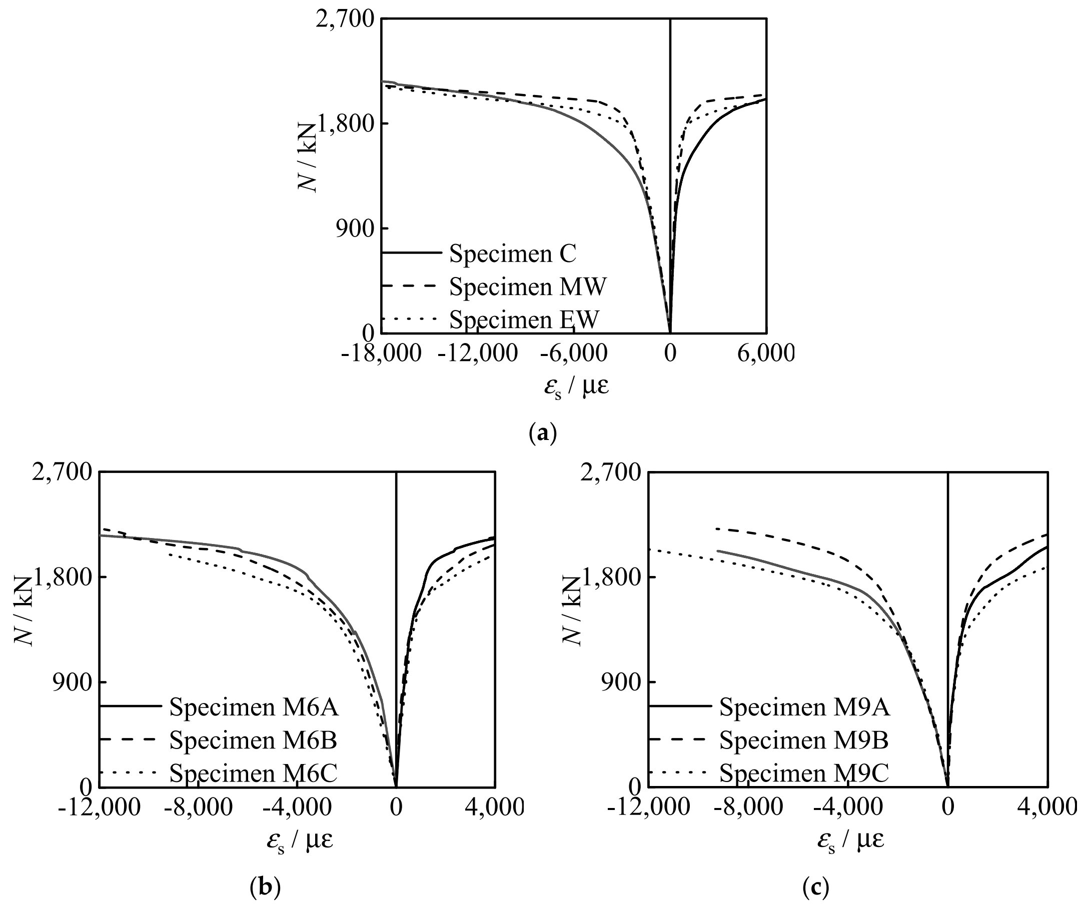

Figure 15. *Cont.*

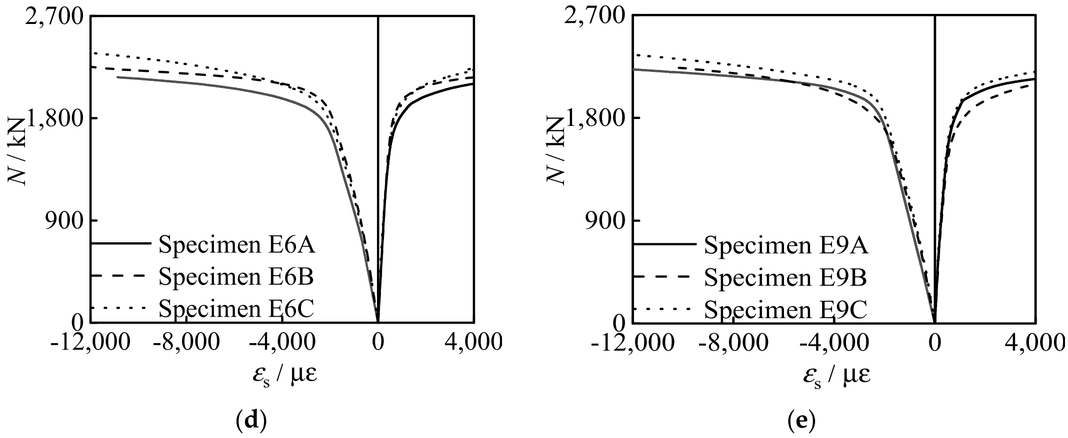

Figure 15. N-ε_s curves of all specimens. (**a**) unconnected specimens; (**b**) middle-section specimens, h = 0.6 mm; (**c**) middle-section specimens, h = 0.9 mm; (**d**) end-section specimens, h = 0.6 mm; (**e**) end-section specimens, h = 0.9 mm.

5. Analysis of Influencing Factors

5.1. Thread Length

Figure 16 shows the effect of thread length on the N-Δ curves. The length of the thread is proportional to the bearing capacity. This is because the longer the thread, the longer the length of the inner liner and the greater the constraint effect of the thread section on the concrete, which has a certain strengthening effect on the stiffness and bearing capacity of the test piece. This indicates that such connections do not weaken the strength of axially compressed stub columns.

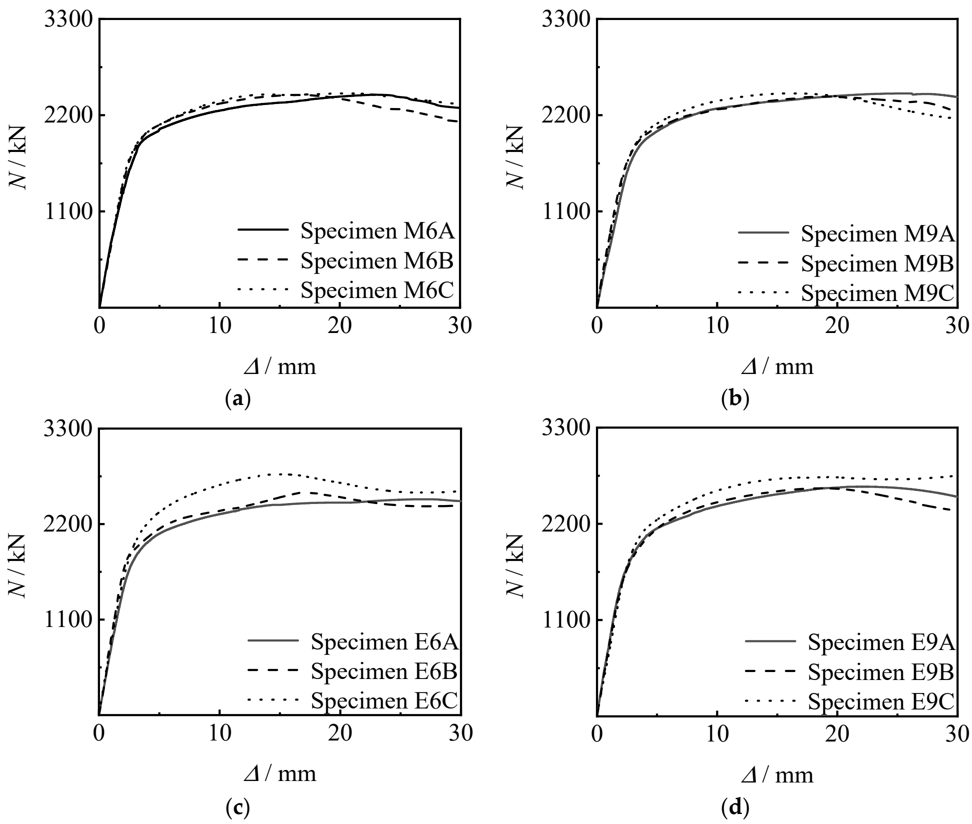

Figure 16. Effect of thread length on N-Δ curves of connected specimens. (**a**) middle-section specimens, h = 0.6 mm; (**b**) middle-section specimens, h = 0.9 mm; (**c**) end-section specimens, h = 0.6 mm; (**d**) end-section specimens, h = 0.9 mm.

5.2. Thread Position

Figure 17 shows the influence of thread position on the *N*-Δ curve of the specimen. Compared to the mid-section connection specimen, the end-section connection specimen has a better constraint effect on concrete, therefore the macroscopic performance is as follows: the end connections have a greater impact on the bearing capacity of the specimen [24,25].

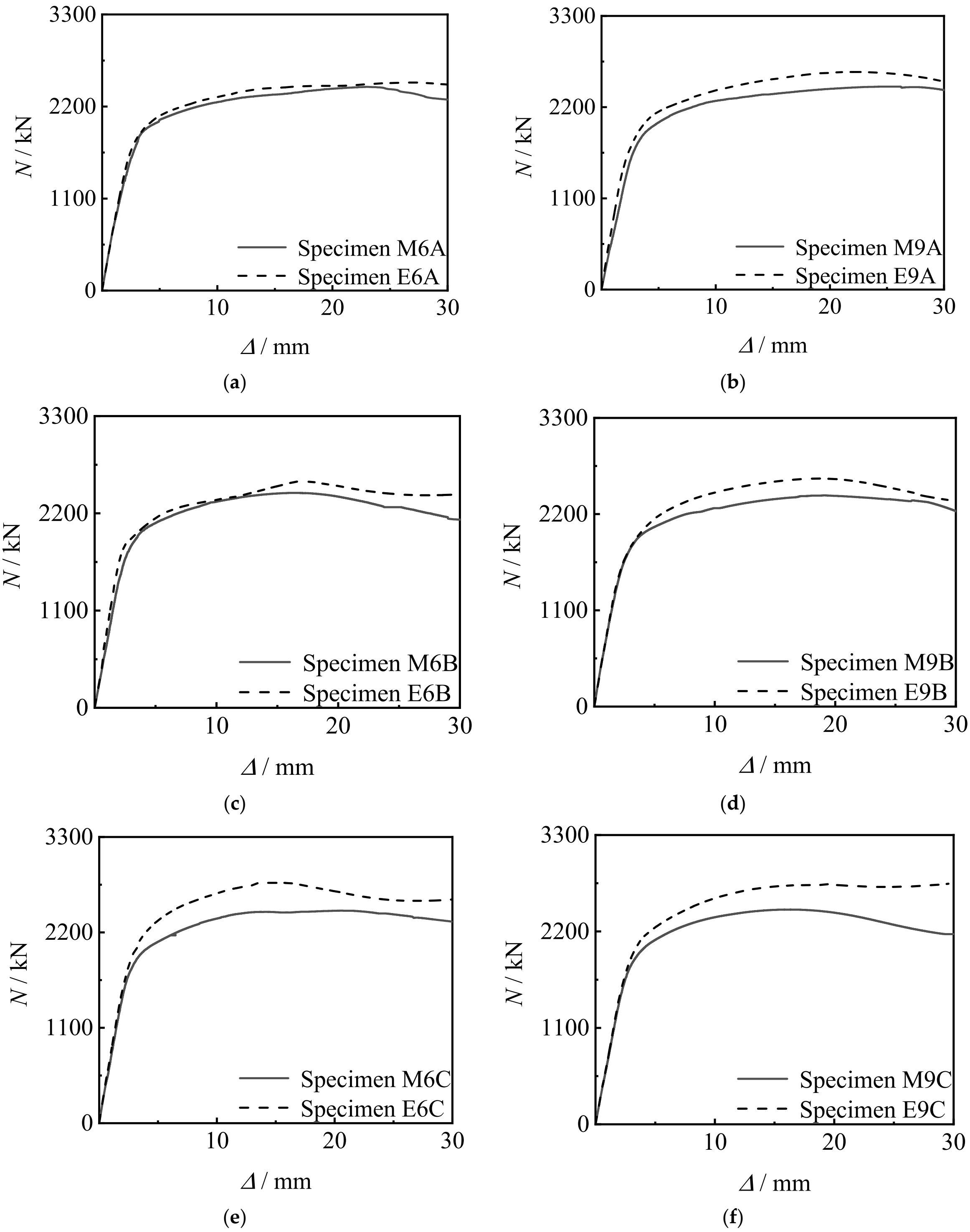

Figure 17. Effect of thread position on *N*-Δ curves of connected specimens. (**a**) Specimens h = 0.6 mm, l = 16.5 mm; (**b**) Specimens h = 0.9 mm, l = 33 mm; (**c**) Specimens h = 0.6 mm, l = 66 mm; (**d**) Specimens h = 0.9 mm, l = 16.5 mm; (**e**) Specimens h = 0.6 mm, l = 33 mm; (**f**) Specimens h = 0.9 m, l = 66 mm.

5.3. Thread Depth

Figure 18 shows the influence of thread depth on the *N*-Δ curve of the specimen. The thread depth parameters of the specimen this time are 0.6 mm and 0.9 mm, respectively. The difference between the two thread depths is small, so the impact on the increase in bearing capacity is not significant.

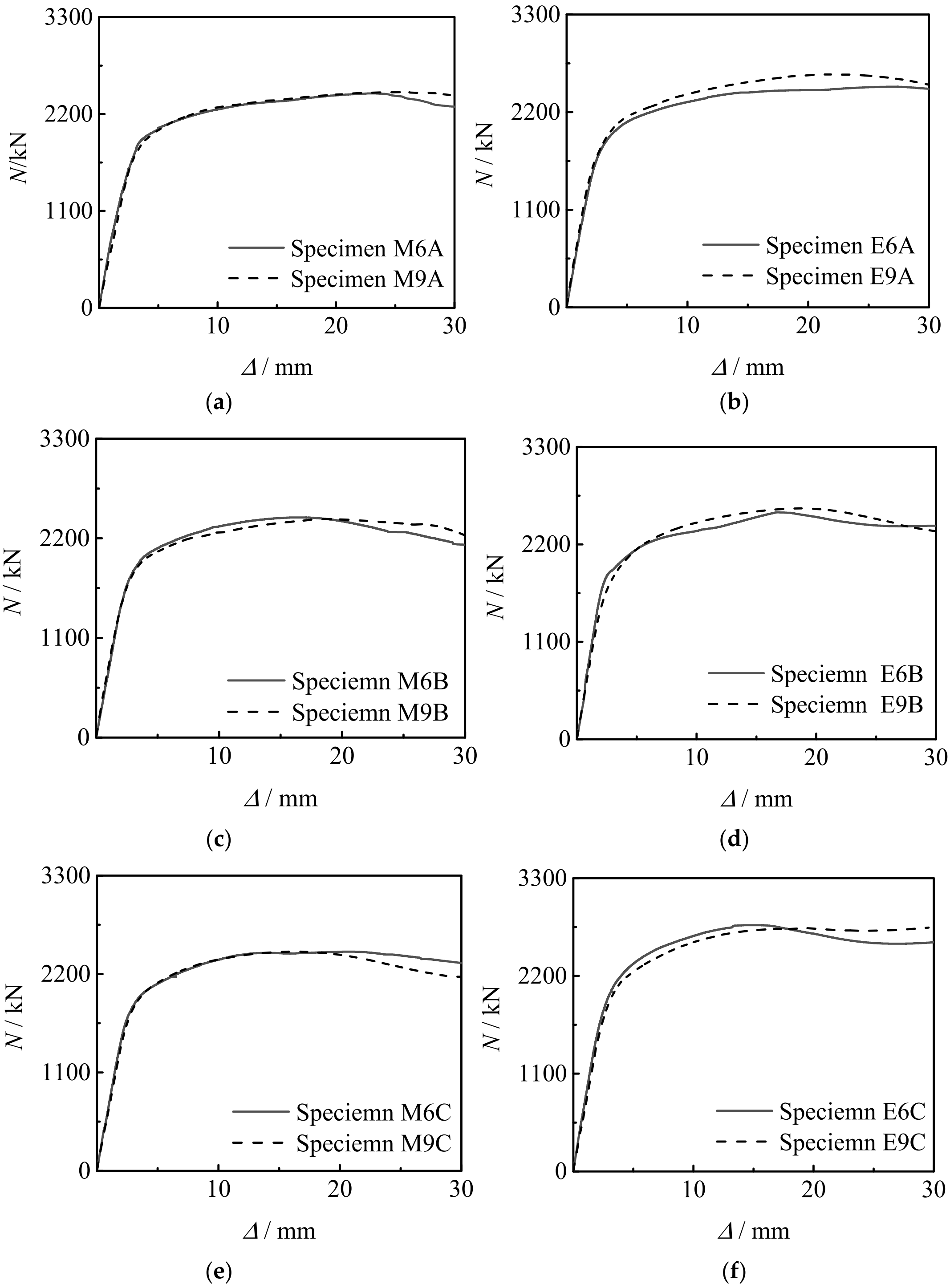

Figure 18. Effect of thread depth on *N*-Δ curves of connected specimens. (**a**) middle-section specimens, *l* = 16.5 mm; (**b**) end-section specimens, *l* = 16.5 mm; (**c**) middle-section specimens, *l* = 33 mm; (**d**) end-section specimens, *l* = 33 mm; (**e**) middle-section specimens, *l* = 66 mm; (**f**) end-section specimens, *l* = 66 mm.

6. Calculation of Load Bearing Capacity

In order to reasonably determine the axial compressive strength-bearing capacity of hollow concrete-filled sandwich circular steel tube specimens, the relationship between N-ε_s and N-Δ curves are studied, and the loading value is defined as N_{ue} when the strain of the specimen reaches 6500 με. The basis is as follows: first, when the strain is 6500 με, the elasto-plastic stage of the specimen basically ends, but it does not reach the plastic stage. Second, the steel tube and concrete basically reach the limit state, and the concrete reaches the limit stress at 6500 με. Finally, the strain increases slowly, while the loading increases rapidly before 6500 με; and after 6500 με, the loading increases relatively slowly with the rapid increase of strain [26,27].

According to academic, European, American, and Chinese standards, the results obtained from the calculation expressions for the bearing capacity of circular hollow sandwich steel tube concrete short columns under axial compression are compared with the experimental results in this paper. The calculation formulas are shown in Equations (4)–(11). The recommended formula for calculating the axial compressive bearing capacity of circular sleeve circular hollow sandwich steel tube concrete columns in the Society's standard T/CCES 7-2020 "Technical Specification for Hollow Sandwich Steel Tube Concrete Structures" is [17]:

$$N = N_{osc,u} + N_{i,u} = f_{scy} A_{sco} + f_{si} A_{si} \tag{4}$$

$$A_{sco} = A_{so} + A_c \tag{5}$$

where $N_{osc,u}$ is the cross-sectional compressive bearing capacity of the outer steel pipe and the sandwich concrete; $N_{i,u}$ is the cross-sectional compressive-bearing capacity of the inner steel pipe; A_{so}, A_c is the cross-sectional area of outer steel pipe and sandwich concrete and f_{scy} is the strength index of hollow sandwich steel pipe concrete.

The formula recommended by the European Committee for Standardization EN 1994-1-1 (2004) for calculating the axial compressive-bearing capacity of circular hollow sandwich steel tube concrete columns with circular sleeves is as follows [28]:

$$N = \eta_{a0} f_{yo} A_{so} + f_c A_c \left[1 + \eta_{c0} \cdot (\mathrm{t}/\mathrm{d}) \cdot \left(f_y / f_{ck}\right)\right] + f_{yi} A_{si} \tag{6}$$

$$\eta_{a0} = 0.25(3 + 2\lambda) < 1.0 \tag{7}$$

$$\eta_{c0} = 4.9 - 18.5\lambda + 17\lambda^2 \geq 0 \tag{8}$$

where f_{yo}, f_{yi} is the yield strength of outer and inner steel pipes, respectively; A_{so}, A_c is the cross-sectional area of outer and inner steel pipes, respectively; f_c is the design value of concrete compressive strength; and A_c is the cross-sectional area of sandwich concrete.

The formula for calculating the axial compressive bearing capacity of circular hollow sandwich steel tube concrete columns recommended by the American Steel Structure Code ANSI/AISC 360-16 is as follows [29]:

$\lambda \leq \lambda_p$:

$$N = f_{yo} A_{so} + 0.95 f_c A_c + f_{yi} A_{si} \tag{9}$$

$\lambda_p < \lambda \leq \lambda_r$:

$$N = f_{yo} A_{so} + 0.95 f_c A_c - 0.25 \left(\frac{\lambda - \lambda_p}{\lambda_r - \lambda_p}\right)^2 \cdot f_c A_c + f_{yi} A_{si} \tag{10}$$

where f_{yo}, f_{yi} is the yield strength of outer and inner steel pipes, respectively; A_{so}, A_c is the cross-sectional area of outer and inner steel pipes, respectively; f_c is the design value of concrete compressive strength; and A_c is the cross-sectional area of sandwich concrete.

The formula recommended by the Chinese standard GB 50936-2014 "Technical Specification for Concrete Filled Steel Tubular Structures" for calculating the axial compressive-bearing capacity of circular sleeve hollow sandwich steel tube concrete columns is [30]:

$$N = f_{sc}A_{sc} + f_{si}A_{si} \tag{11}$$

where f_{sc} is the design value of compressive strength of hollow sandwich steel pipe concrete; A_{sc} is the sum of the cross-sectional areas of the outer steel pipe and concrete; and A_{si}, A_s is the cross-sectional area of the inner and outer steel pipes, respectively.

The calculated results based on the calculation expression of the axial compressive-bearing capacity of hollow concrete-filled sandwich circular steel tubular specimens in different references are compared with the test results. The comparison results are shown in Table 3, where N_{ue} is the test value and N_{uc} is the calculated value. It can be seen that the calculated results based on the calculation equations proposed in [17,28,29] agree well with the test values.

Table 3. Comparison of calculation and test values of bearing capacity.

No.	Test Values N_{ue}/kN	N_{uc}/N_{ue} Reference [17]	Reference [28]	Reference [29]	Reference [30]
M6A	2040	0.93	0.91	0.91	0.77
M6B	2090	0.90	0.89	0.89	0.75
M6C	2091	0.90	0.89	0.89	0.75
M9A	2017	0.94	0.92	0.92	0.78
M9B	2053	0.92	0.91	0.90	0.77
M9C	2105	0.90	0.89	0.88	0.75
E6A	2088	0.90	0.89	0.89	0.76
E6B	2146	0.88	0.87	0.86	0.73
E6C	2337	0.81	0.80	0.79	0.67
E9A	2147	0.88	0.87	0.86	0.73
E9B	2150	0.88	0.87	0.86	0.73
E9C	2245	0.84	0.83	0.83	0.70
Average value		0.89	0.88	0.87	0.74
Standard deviation		0.036	0.034	0.036	0.031

7. Conclusions

(1) The initial stage of the axial compressive loading–longitudinal compressive displacement curves of the hollow concrete-filled sandwich circular steel tubular specimens is the elastic stage, and the relationship between loading and displacement is linear. After that, the curves enter the elasto-plastic stage. With the gradual increase of displacement, the curves enter the yield-strengthening stage. After reaching the peak load, the load begins to drop, and curves enter the descending stage.

(2) The bearing capacity and stiffness of the specimens connected by thread through the inner lining tube are not inferior to the welded specimen or the ordinary specimen.

(3) The bearing capacity and stiffness of the specimens connected by thread through the inner lining tube increase with the increase of the thread length.

(4) By comparing the corresponding references, the calculations of the axial compressive bearing capacity are suggested.

Author Contributions: Conceptualization, Q.W.; Methodology, Q.W.; Software, Q.W. and J.Z.; Validation, K.P.; Formal analysis, J.Z.; Investigation, J.Z.; Resources, J.Z.; Data curation, Q.W.; Writing—review and editing, K.P.; Visualization, K.P.; Supervision, K.P.; Project administration, K.P. All authors have read and agreed to the published version of the manuscript.

Funding: This research was funded by Project for Talent of Liaoning Province (No. XLYC1902009).

Data Availability Statement: The datasets used or analyzed during the current study are available from the corresponding author on reasonable request.

Conflicts of Interest: The authors declare no conflict of interest.

References

1. Wei, S.; Mau, S.T.; Vipulanandan, C. Performance of new sandwich tube under axial loading: Analysis. *J. Struct. Eng. ASCE* **1995**, *121*, 1815–1821. [CrossRef]
2. Zhao, X.L.; Grzebieta, R.H.; Ukur, A.; Elchalakani, M. Tests of concrete-filled double skin (SHS outer and CHS inner) composite stub columns. In Proceedings of the Third International Conference on Advances in Steel Structures, Hong Kong, China, 9–11 December 2002; Volume I, pp. 567–574.
3. Ci, J.; Ahmed, M.; Liang, Q.Q.; Chen, S.; Chen, W.; Sennah, K.; Hamoda, A. Experimental and numerical investigations into the behavior of circular concrete-filled double steel tubular slender columns. *Eng. Struct.* **2022**, *267*, 114644. [CrossRef]
4. Dong, L.; Zhang, W.L. Ultimate compressive capacity of tapered concrete-filled double skin steel tubular stub columns with large hollow ratio. *J. Constr. Steel Res.* **2022**, *196*, 107356.
5. Thang, V.; Marshall, P. Studded bond enhancement for steel-concrete-steel sandwich shells. *Ocean. Eng.* **2015**, *15*, 31–39. [CrossRef]
6. Ahmed MM, Z.; El-Sayed Seleman, M.M.; Touileb, K.; Albaijan, I.; Habba, M.I.A. Microstructure, crystallographic texture, and mechanical properties of friction stir welded mild steel for shipbuilding applications. *Materials* **2022**, *15*, 2905. [CrossRef] [PubMed]
7. Yan, L.S.; Wei, X.W.; Wang, H.; Wei, B. Mechanical behaviour of circular steel-reinforced concrete-filled steel tubular members under pure bending loads. *Structures* **2020**, *112*, 8–25.
8. Jiang, S.C.; Wang, Z.; Zhao, X.L. Structural performance of prestressed grouted pile-to-sleeve connection. *J. Constr. Steel Res.* **2023**, *201*, 107689. [CrossRef]
9. Sun, W.-b. Experimental study grouting concrete filled steel tube column sleeve connection capacity. *Eng. Struct.* **2022**, *267*, 114600. [CrossRef]
10. Wang, W.-d.; Yi, L.-b.; Fan, J.-h. Analysis of bending performance of inner and outer flange connections of circular concrete-filled double skin steel tubular (CFDST) member. *J. Archit. Civ. Eng.* **2020**, *37*, 42–51.
11. Yi, L.-b. Research on mechanical properties of inner and outer flange connections of tapered concrete-filled double skin steel tube members. *J. Lanzhou Univ. Technol.* **2020**, *6*, 77–81.
12. Deng, H.; Song, X.; Chen, Z.; Fu, P.; Dong, J. Experiment and design methodology of a double-layered flange connection in axial loads. *Eng. Struct.* **2018**, *175*, 436–456. [CrossRef]
13. Grundy, P.; Kiuj, F. Prestress enancement of grouted pile/sleeve connections. In Proceedings of the First International Offshores and Polar Engineering Conference, ISOPE, Edinburgh, UK, 11–16 August 1991; Volume 1, pp. 130–136.
14. Zhai, S.-s. Study on axial compression performance of concrete filled steel tubular columns with inner casing connections. *J. Zhongyuan Univ. Technol.* **2018**, *7*, 18–99.
15. Yang, H.; Yu, Y.; Kang, L.; Chen, J.; Luo, Y. Research on the mechanical behavior of flange connected concrete filled steel tubular column-steel beam reinforced ring joints. *J. Build. Struct.* **2022**, *43*, 157–162.
16. Wang, J.; Chen, J. The effect of connection methods on the axial tensile properties of concrete-filled steel tubular members with internal lattice angle steel. *J. Build. Struct.* **2019**, *40*, 354–361.
17. Lei, Y.; Ling, Z. Study on stainless steel blind bolted T-stub to concrete-filled stainless steel tube connections. *Eng. Struct.* **2022**, *257*, 114107. [CrossRef]
18. *DBJ/T 13-51-2020*; Technical Specification for Concrete-Filled Double Skin Steel Tubular Structures. China Architecture & Building Press: Beijing, China, 2020.
19. Tao, Z.; Yu, Q. *New Composite Structural Column—Experiment, Theory and Method*; Science Press: Beijing, China, 2006.
20. Huang, H. Performance analysis of hollow sandwich concrete filled steel tubular short columns. *Structures* **2010**, *25*, 81–82.
21. Su, H.T.; Han, F.X. Experimental study on axial compression of circular hollow sandwich steel tube self compacting concrete short columns based on changes in void fraction. *Concrete* **2018**, *7*, 13–18.
22. Wang, Z.B.; Guo, J. Research on the axial compression performance of hollow sandwich thin-walled steel tube concrete short columns. *Prog. Build. Steel Struct.* **2020**, *20*, 7.
23. Cong, S.P.; Peng, M. Axial compression performance test of square hollow sandwich steel tube concrete short columns. *Chin. Sci. Technol. Pap.* **2019**, *14*, 1085–1089.
24. Ni, G. Analysis of axial compression performance of hollow sandwich steel tube concrete columns with outer circle and inner square. *Low Temp. Build. Technol.* **2019**, *41*, 5–10.
25. Xu, P.; Liu, Q. Experimental study on axial compression of circular hollow sandwich steel pipe self compacting concrete short columns based on changes in diameter to thickness ratio. *Concrete* **2019**, *6*, 10–19.
26. Yan, X.F.; Zhao, Y.G. Compressive strength of axially loaded circular concrete-filled double-skin steel tubular short columns. *J. Constr. Steel Res.* **2020**, *170*, 106–114. [CrossRef]
27. Tao, Z.; Han, L.H.; Zhao, X.L. Behaviour of concrete-filled double skin (CHS inner and CHS outer) steel tubular stub columns and beam-columns. *J. Constr. Steel Res.* **2004**, *60*, 1129–1158. [CrossRef]

28. *EN 1994-1-1:2004*; Design of Composite Steel and Concrete Structures-Part1-1: General Rules and Rules for Buildings: Eurocode 4. European Committee for Standardization: Brussels, Belgium, 2004.
29. *ANSI/AISC 360-16*; Specification for Structural Steel Buildings. American Institute of Steel Construction: Chicago, IL, USA, 2016.
30. *GB 50936-2014 (GB50936-2014)*; Technical Code for Concrete Filled Steel Tubular Structures. China Architecture & Building Press: Beijing, China, 2014.